State-dependence of the equilibrium climate sensitivity in a clear-sky GCM

Matthew Henry[1], Geoffrey K. Vallis[1], Nicholas J. Lutsko[2], Jacob T. Seeley[3], and Brett A. McKim[1,4]

[1]Department of Mathematics, University of Exeter, Exeter, UK
[2]Scripps Institution of Oceanography, La Jolla, California, USA
[3]Department of Earth and Planetary Sciences, Harvard University, USA
[4]LMD/IPSL, Sorbonne Université, CNRS, Paris, France

Corresponding author: Matthew Henry, m.henry@exeter.ac.uk

Abstract

Climate sensitivity peaks around 310K in a wide variety of climate models, ranging from idealized single column models to fully comprehensive climate models. Although an explanation for this peak has been developed using single column models with fixed relative humidity and line-by-line radiation, the relevance of this theory for explaining the peak in comprehensive climate models is unclear. In this paper we increase CO_2 using a clear-sky 3-dimensional climate model with a radiation scheme that maintains accuracy for high CO_2 and temperature levels. The Equilibrium Climate Sensitivity (ECS) of our model shows a plateau around 310K with the moistening of the subtropical regions caused by a slowdown in atmospheric circulation increasing the ECS at very high CO_2 values. Though the changes in CO_2 and temperature presented here are extreme, this study shows the potential importance of changes in atmospheric circulation and relative humidity in quantitative assessments of climate sensitivity.

1 Introduction

Equilibrium Climate Sensitivity (ECS) is defined as the amount by which surface temperature changes after a doubling of CO_2 and when equilibrium has been reached. That equilibrium is somewhat ill-defined, and there is both paleoclimate (Anagnostou et al., 2020) and climate model evidence (Bloch-Johnson et al., 2021) that the ECS is state-dependent and increases at higher temperature. Moreover, Bloch-Johnson et al. (2021) found that, for almost all models from the Sixth Coupled Model Intercomparison Project (CMIP6), the clear-sky longwave feedback is less stabilizing at high temperatures, whereas there is no such agreement for the other components of the climate feedback. This can be understood to be a consequence of the closing of the atmospheric water vapor window (Koll & Cronin, 2018).

By systematically increasing either the solar constant or greenhouse gas concentrations, a peak in ECS has been found around 310K in a variety of climate models spanning the climate model hierarchy (e.g., Leconte et al., 2013; Meraner et al., 2013; Russell et al., 2013; Wolf & Toon, 2015; Popp et al., 2016; Wolf et al., 2018; Romps, 2020). However, Kluft et al. (2021) show that an out-of-bounds use of comprehensive climate model radiation schemes can lead to an erroneously large peak in ECS, and that may explain the much larger peaks in ECS in comprehensive climate models compared to single-column calculations with more accurate radiation schemes by Kluft et al. (2021) and Seeley and Jeevanjee (2021). Both studies show a peak in ECS of around 5 K at approximately 310 K when CO_2 is increased. Seeley and Jeevanjee (2021) show that the peak in ECS is due to a competition between the closing of the water vapor window and the opening of the CO_2 radiator fins, but this explanation only applies to a world warmed by increasing CO_2, rather than increasing the solar constant, and only to an atmosphere in radiative-convective equilibrium.

This clear-sky explanation for the peak in ECS is based on a single column model with constant relative humidity. Zhang et al. (2020) analyse comprehensive climate model simulations and show the importance of having a constant relative humidity distribution in order to have a constant clear-sky longwave feedback. Bourdin et al. (2021) use a radiative-convective single column model to show that the vertical structure of relative humidity also affects the clear-sky longwave feedback. This vertical dependence can be explained by the emission level theory for longwave emission: if the relative humidity is more bottom-heavy, there is more of an increase in emitters below the emission level, hence pushing the emission level down, and decreasing the climate's sensitivity. This previous work suggests that both the climatological relative humidity and any changes to the relative humidity distribution will play an important role in shaping the clear-sky longwave feedback.

In this work, we analyze a range of climates using a clear-sky configuration of Isca (Vallis et al., 2018), with a comprehensive radiation scheme that maintains good accuracy for atmospheres with up to 10% CO_2 by volume (i.e., 100,000 ppm) and 500 K. This provides a connection between the single column model with line-by-line radiation computation (Seeley & Jeevanjee, 2021; Kluft et al., 2021) and more comprehensive 3-dimensional GCMs. In particular, it enables us to

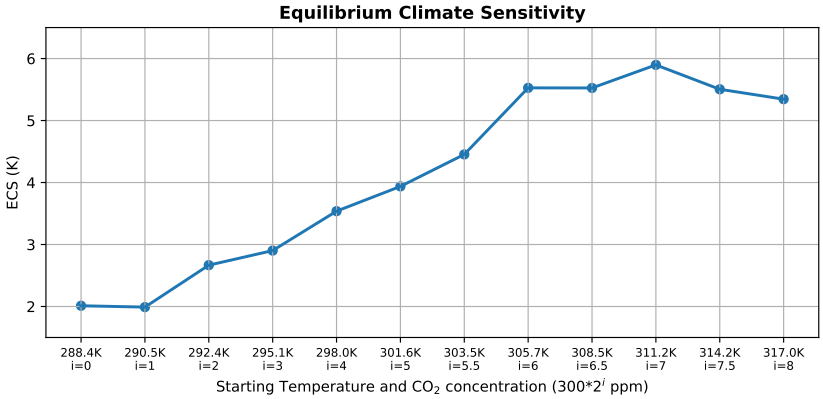

Figure 1. Equilibrium Climate Sensitivity (ECS) for the suite of clear-sky GCM simulations. The CO_2 concentration is set to 300ppm$\times 2^i$.

analyze how radiation and changes in relative humidity affect the clear-sky longwave feedback. We first describe the model and experiments. Second, we describe the changes in the atmospheric energy transport and relative humidity, then analyze how changes in relative humidity affect the radiative feedback. Finally, we confirm our understanding through a latitudinal decomposition of the relative humidity and feedback.

2 Model and experimental description

We increase CO_2 in a clear-sky aquaplanet configuration of the Isca climate modeling framework (Vallis et al., 2018), here configured with no sea ice, a slab ocean boundary condition, no land or topography, a hydrology cycle but no clouds, and annual-mean insolation. We use the comprehensive SOCRATES radiation scheme for infra-red and solar radiation (Manners et al., 2017; Thomson & Vallis, 2019), and this maintains good accuracy for up to 10% CO_2 and 500 K. The surface albedo is set uniformly to 0.15. Simulations are run at spectral T42 resolution, which corresponds to approximately 2.8 degrees resolution at the equator. Convection is calculated using a simplified Betts-Miller convection scheme (Frierson, 2007). Large scale condensation is parameterized such that relative humidity does not exceed one, and condensed water immediately returns to the surface. Popp et al. (2016) found that removing stratospheric ozone may affect upper atmospheric levels of moisture but makes no substantial difference to the surface climate, and Wolf and Toon (2015) and Leconte et al. (2013) do not include ozone in their simulations. We hence choose not to include stratospheric ozone.

We perform experiments in which CO_2 concentration is variously set to 300 ppm, 600 ppm, 1200 ppm, 2400 ppm, 4800 ppm, 9,600 ppm, 9,600 ppm $\sqrt{2}$, 19,200 ppm, 19,200 ppm $\sqrt{2}$, 38,400 ppm, 38,400 ppm $\sqrt{2}$, 76,800 ppm, and 76,800 ppm $\sqrt{2} \approx$ 101,000 ppm for 100 months each successively. We include simulations with $\sqrt{2}$ increases in the concentration of CO_2 in order to give a more uniform resolution of ECS values around the 310 K peak in global-mean surface temperature (GMST). In what follows, the CO_2 concentration will be expressed as 300 ppm $\times 2^i$ with i=[0, 1, 2, 3, 4, 5, 5.5, 6, 6.5, 7, 7.5, 8, 8.5]. The simulations all reach an equilibrium after approximately 30 months as the net TOA radiation reaches zero and the surface temperature stabilizes. Figure 1 shows the equilibrium climate sensitivity for each increase in CO_2. Given that the forcing increases approximately logarithmically with CO_2 concentration, if the increase in CO_2 concentration is a multiplication by $\sqrt{2}$, then the surface temperature change has been multiplied by two to make it equivalent to a doubling of CO_2. The ECS plateaus at around 305 K in GMST, with a mild maximum at 311 K.

Figure S1 shows the temperature and radiative temperature tendencies of two versions of Isca in single column mode: one with the radiation scheme used in the standard 3-dimensional version of the GCM (17 bands) used for the simulations described above and one with a high resolution radiation scheme (350 bands). The radiative tendencies quantify how each component (radiation, convection, dynamics, etc) of the climate model affects the temperature at a given location and should sum to zero when the simulation reaches equilibrium. Given the close similarity between the two versions of the single column model, we are confident in the validity of the radiation scheme used in the full GCM (i.e. the 17 band scheme). We thus avoid the problem of an out-of-bounds use of a GCM radiation scheme, which can leads to an erroneously large peak in ECS, as was found in other comprehensive GCMs (Kluft et al., 2021).

3 Atmospheric energy transport and relative humidity changes

Figure 2 shows the relative humidity, atmospheric energy transport, streamfunction, and atmospheric temperature for the 300 ppm, 78600 ppm, and 115200 ppm simulations. The total atmospheric energy transport is calculated as the vertical integral of the net energy fluxes into the atmosphere, and the moist component is calculated as the integral of evaporation minus precipitation times the latent heat of vaporisation. The latitudinal gradients of $C_p T_S$ and Lq are shown in Figure S2, where C_p is the heat capacity of air at constant pressure, T_S is the surface temperature, L is the latent heat of vaporization, and q is the near-surface specific humidity. The decrease of the latitudinal gradient of $C_p T_S$ and increase of that of Lq in the extratropics are consistent with Figure 2.

The tropical tropopause height (between 30 degrees North and South) can be estimated by where the radiative cooling rate first goes to zero (Seeley et al., 2019). In the tropics where the atmosphere is in radiative-convective equilibrium, we can equally use the convective criterion, whereby the tropopause is set to where the convective temperature tendency goes below 0.01 K/day. There is a slight difference due to the presence of atmospheric energy export, but this does not meaningfully affect the results. The tropopause is also commonly computed using a 2K/km lapse rate threshold. Both tropopause calculations are shown in the temperature and streamfunction panels. Figure S3 shows the lapse rate and convective tropopause pressure and temperature for all simulations. As expected the tropopause goes up in height for all latitudes, but its temperature decreases in the tropics and increases in the extratropics using the 2K/km lapse rate threshold (fig. S3), but stays roughly constant when using the convective criterion. The choice of the 2K/km threshold value works for present-day Earth but should not be expected to apply to these idealized very high CO_2 atmospheres. That the fixed tropopause temperature hypothesis does not fully hold in the tropics is expected as that hypothesis assumes radiative effects are dominated by water vapor, whereas CO_2 concentrations are taken to extreme values in these simulations.

Four key changes are occurring simultaneously in our simulations: a slowdown of atmospheric circulation (weaker streamfunction, see fig. 2g,h, and i), an increase in the tropopause height, an increase in the moist component of atmospheric energy transport in the extratropics, and a moistening of the subtropics. The increase in tropopause height is expected as the surface temperature increases (Hu & Vallis, 2019; Seeley et al., 2019). The general slowdown of the circulation may be attributed to an increase in the moist contribution to the overall energy transport, thus requiring a weaker overall circulation. Given a weaker circulation (and less intense Hadley Cell) a moistening of the subtropics can be expected (Pierrehumbert et al., 2007; Vallis, 2017). However, a fuller and more quantitative exploration of these effects requires future study.

4 Role of relative humidity distribution change

We now seek to understand the role of relative humidity change in the ECS peak. The forcing, feedback, and temperature change are related by: $F + \lambda \Delta T_S = 0$, where F is the top-of-atmosphere forcing (namely, the instantaneous change in the top-of-atmosphere radiative balance), ΔT_S is the change in surface temperature, and λ is (to use the conventional term) the feedback. The feedback (λ) can be calculated as the difference in top-of-atmosphere radiation of two sim-

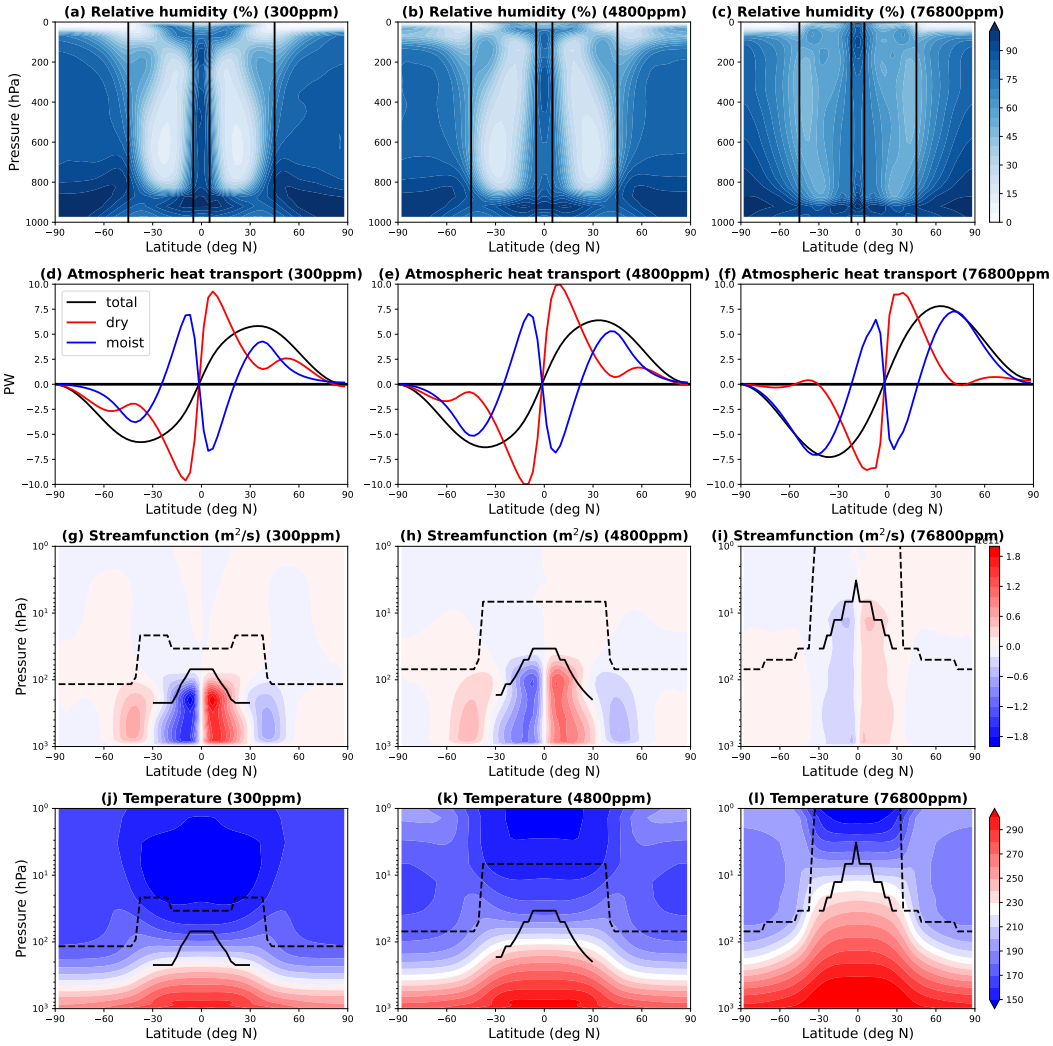

Figure 2. Relative humidity (a,b,c), atmospheric energy transport (d,e,f), streamfunction (g,h,i), and temperature (j,k,l) for the 300ppm (a,d,g,j), 36400ppm (b,e,h,k), and 115200ppm (c,f,i,l) simulations. Note that the y-axis in panels g-l are in log scale. The solid black line in panels g-l is an estimation of the tropical tropopause using a convective criterion. The dashed black line in panels g-l is the thermal tropopause, defined by the height at which the lapse rate goes below 2K/km. The pressure and temperature of the tropopause as computed by the two methods is shown in Figure S3.

ulations: one with fixed control surface temperature and one with the surface temperature increased by one degree from the control. When calculated in this way, the atmospheric temperature and specific humidity are allowed to increase and thus affect the TOA radiation budget. In order to isolate the effects of changes in relative humidity on the feedback, we calculate the feedback in a different but equivalent manner. Between two equilibrated climates, the top-of-atmosphere forcing F is balanced by changes in the outgoing longwave radiation (OLR) and top-of-atmosphere net shortwave radiation (SW) such that $F + \Delta SW + \Delta OLR = 0$. The change in OLR is then separated into changes caused by surface temperature, atmospheric temperature, and specific humidity respectively, as follows:

$$\underbrace{F + \Delta SW + \Delta OLR|_{\delta T_S \text{ and } T_a, SH\text{fixed}} + \Delta OLR|_{\delta T_a \text{ and } T_S, SH\text{fixed}} + \Delta OLR|_{\delta SH \text{ and } T_S, T_a\text{fixed}}}_{\lambda \Delta T_S} = 0. \quad (1)$$

Here, $\Delta OLR|_{\delta T_S \text{ and } T_a, SH\text{fixed}}$ is the change in OLR when surface temperature is increased to the higher CO_2 simulation's surface temperature (not increased only by 1 K) and the atmospheric temperature (T_a) and specific humidity (SH) are kept fixed, the next two terms similarly consider the effect of changes in atmospheric temperature (T_a) and specific humidity (SH) in isolation, and ΔSW is the change in TOA shortwave radiation. The global mean of each of these terms is shown in Figure 3a for all simulations.

The feedback, λ, is then calculated as:

$$\lambda = \lambda_{SW} + \lambda_{T_S} + \lambda_{T_a} + \lambda_{SH}$$

$$\lambda = \left(\Delta SW + \Delta OLR|_{\delta T_S \text{ and } T_a, SH\text{fixed}} + \Delta OLR|_{\delta T_a \text{ and } T_S, SH\text{fixed}} + \Delta OLR|_{\delta SH \text{ and } T_S, T_a\text{fixed}}\right) / \Delta T_S. \quad (2)$$

The forcing F is calculated as the change in OLR when CO_2 is increased while keeping T_S, T_a, and SH fixed. (We thus neglect the rapid adjustments which are often included in forcing estimates.) The feedback calculated as $F/\Delta T_S$ is shown in Figure 3b (black) and is compared to the feedback calculated as shown in equation 2 (blue).

To estimate the impact of changes in relative humidity on the feedback, we recalculate it assuming no change in relative humidity. Hence, we multiply the specific humidity at each CO_2 level i (SH_i) by RH_{300ppm}/RH_i, where RH_i is the relative humidity of the given simulation and RH_{300ppm} is the relative humidity of the control 300ppm simulation, and then calculate the feedback. This enables us to approximate how the changes in RH affect the feedback. The impact of this change on the TOA response is shown in Figure 3a (magenta) and shows a weaker water vapor feedback for the high CO_2 simulations, which is reflected in the feedback (fig. 3b) and the ECS (fig. 3c).

The picture that emerges from the simulations is one in which a slowdown in atmospheric circulation causes a moistening of the subtropics, which radiate less efficiently to space (Pierrehumbert, 1995). This then increases the water vapor feedback and climate sensitivity at high CO_2 levels. Ignoring this moistening, and calculating the ECS calculated using a fixed relative humidity (magenta in fig. 3c) results in a sharper peak at i=6, which is more consistent with single column model simulations with comprehensive radiation and fixed relative humidity (Seeley & Jeevanjee, 2021; Kluft et al., 2021).

5 Latitudinal decomposition of changes in relative humidity and feedback

In order to verify our hypothesis that the higher ECS (relative to the fixed relative-humidity ECS) for levels of CO_2 larger than $300\text{ppm} \times 2^6$ is caused by the moistening of the subtropics, we

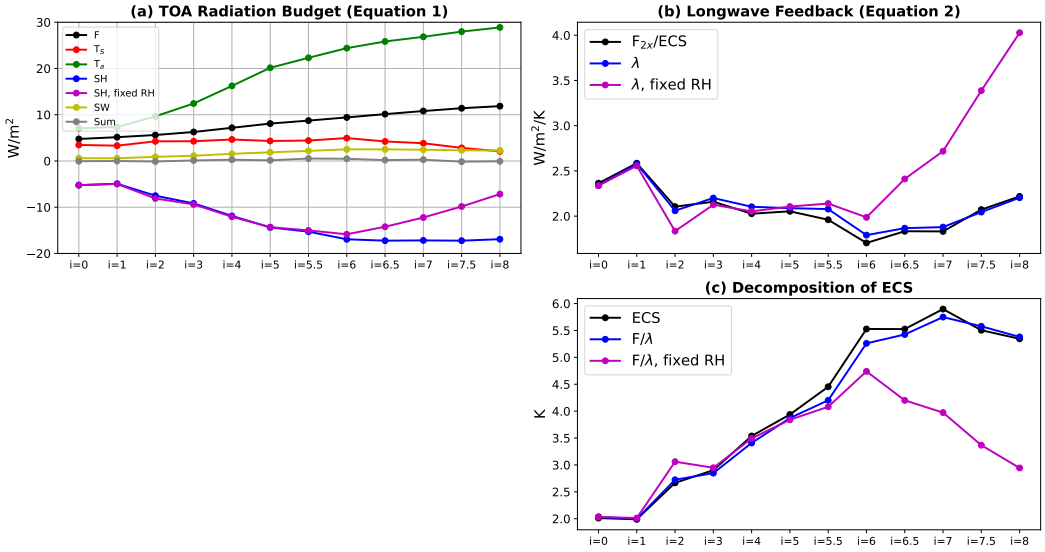

Figure 3. (a) TOA budget terms from Equation 1. (b) Longwave feedback computed using Equation 2, and with assumption of fixed relative humidity (magenta). (c) ECS recalculated with assumption of fixed relative humidity (magenta).

decompose the change in relative humidity and the terms of Eq. (1) according to their latitude. Figure 4 shows the vertical structure of relative humidity between 0 and 40 degrees North (a) and between 40 and 90 degrees North (c), and the corresponding terms of Equation 1 (b,d). The averaged tropics and subtropics see a clear increase in relative humidity from around 40% to around 65% (fig. 4a), whereas there is only a modest decrease in relative humidity poleward of 40 degrees North (fig. 4c). The effect on the feedback can be deduced from the difference between the water vapor feedback term (SH, in blue) in Eq. (1) and the fixed relative humidity water vapor feedback term (SH, fixed RH, in magenta). In the tropics and subtropics, the moistening of the atmospheric column increases the water vapor feedback (blue) compared to an atmosphere with fixed relative humidity (magenta) (fig. 4b), whereas in the region poleward of 40 degrees North, the water vapor feedback does not change when the relative humidity is fixed (fig. 4d).

6 Summary and Conclusions

A peak in equilibrium climate sensitivity (ECS) has previously been found at around 310 K in a variety of of climate models ranging from a single column model (Seeley & Jeevanjee, 2021; Kluft et al., 2021) to comprehensive climate models (e.g., Wolf & Toon, 2015). The purpose of this paper is to better understand the mechanisms and generality of these results by bridging the gap between the simple clear-sky explanation for the peak in ECS found in single column models and the complicated mechanisms present in comprehensive climate models. Among other things this allows us to look at variations in relative humidity, known to be important factor in determining the clear-sky longwave feedback (Zhang et al., 2020; Bourdin et al., 2021). To this end we use a clear-sky aquaplanet configuration of the Isca climate modelling framework (Vallis et al., 2018) with no sea ice, a slab ocean boundary condition, no clouds, annual-mean insolation, and a radiation scheme for infrared radiation which maintains good accuracy for CO_2 levels up 100,000 ppm and temperatures up to 500 K. As we increase CO_2 from 300 ppm (at 285.4 K) to 101,000 ppm (at 317.8 K), we find that the ECS plateaus around 310 K, with only a mild peak.

The reason for the lack of a sharp peak is that the tropical circulation weakens at very high temperatures, leading to a substantial moistening of the subtropics. To isolate the impact of this

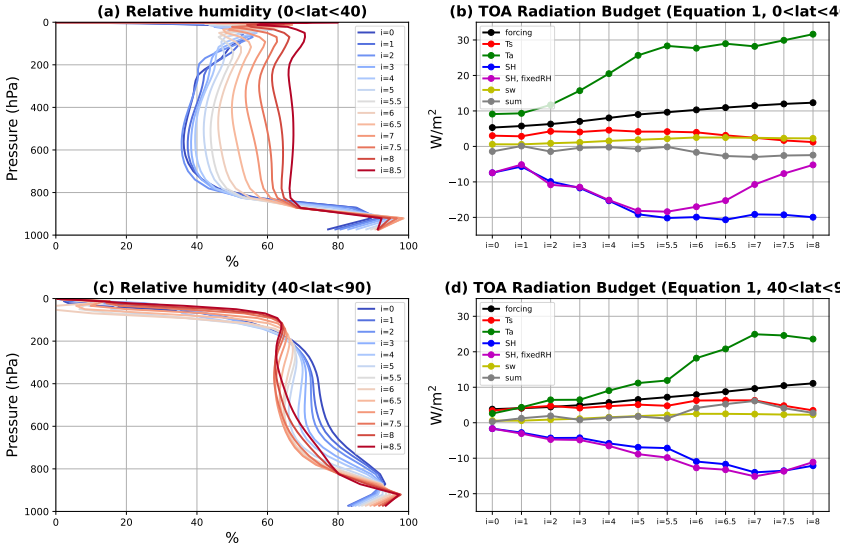

Figure 4. Vertical structure of changes in relative humidity (a,c) and TOA budget terms from Equation 1 (b,d) for latitudes in [0,40] (a,b) and poleward of 40 degrees (c,d).

change in relative humidity on the longwave feedback, we decompose the change in OLR into changes caused by surface temperature, atmospheric temperature, and specific humidity. We then recalculate the feedback assuming no change in relative humidity, and in that case we do find a peak in ECS around 310 K, which is consistent with single column model results (Seeley & Jeevanjee, 2021; Kluft et al., 2021). We then confirm that it is the moistening of the subtropics which causes the increase in ECS by decomposing the feedback and relative humidity by latitude. Evidently, changes in the relative humidity, caused by changes in the circulation, need to be considered in any quantitative theory of climate sensitivity.

Acknowledgments

We wish to thank all the Isca team for many discussions about climate science and modelling, and Nadir Jeevanjee for fruitful discussions. MH and GV were supported by NERC grant number NE/T00942X/1, under a NERC-NSF partnership “Dynamics of Warm Past and Future Climates”. N.J.L was supported by the NOAA Climate Program Office’s Modeling, Analysis, Predictions, and Projections program through grant NA20OAR4310387.

Open Research

The code to reproduce the figures is available at Henry (2023b) and the data is available at Henry (2023a). For the purpose of open access, the author has applied a Creative Commons Attribution (CC BY) licence to any Author Accepted Manuscript version arising.

References

Anagnostou, E., John, E. H., Babila, T., Sexton, P., Ridgwell, A., Lunt, D. J., ... Foster, G. (2020). Proxy evidence for state-dependence of climate sensitivity in the Eocene greenhouse. *Nature communications*, *11*(1), 1–9.

Bloch-Johnson, J., Rugenstein, M., Stolpe, M. B., Rohrschneider, T., Zheng, Y., & Gregory, J. M. (2021). Climate sensitivity increases under higher CO2 levels due to feedback temperature dependence. *Geophysical Research Letters*, *48*(4), e2020GL089074.

Bourdin, S., Kluft, L., & Stevens, B. (2021). Dependence of climate sensitivity on the given distribution of relative humidity. *Geophysical Research Letters*, *48*(8), e2021GL092462.

Frierson, D. M. (2007). The dynamics of idealized convection schemes and their effect on the zonally averaged tropical circulation. *Journal of Atmospheric Sciences*, *64*(6), 1959–1976.

Henry, M. (2023a). *Dataset for "State-dependence of the equilibrium climate sensitivity in a clear-sky GCM" by Matthew Henry et al. (2023).* [Dataset] Zenodo. doi: 10.5281/zenodo.7892332

Henry, M. (2023b). *matthewjhenry/ECS peak paper: Code for "State-dependence of the equilibrium climate sensitivity in a clear-sky GCM" by Henry et al. (2023).* [Software] Zenodo. doi: https://doi.org/10.5281/zenodo.7892355

Hu, S., & Vallis, G. K. (2019). Meridional structure and future changes of tropopause height and temperature. *Quart. J. Roy. Met. Soc*, 1–20. doi: https://doi.org/10.1002/qj.3587

Kluft, L., Dacie, S., Brath, M., Buehler, S. A., & Stevens, B. (2021). Temperature-dependence of the clear-sky feedback in radiative-convective equilibrium. *Geophysical Research Letters*, *48*(22), e2021GL094649.

Koll, D. D., & Cronin, T. W. (2018). Earth's outgoing longwave radiation linear due to H2O greenhouse effect. *Proceedings of the National Academy of Sciences*, *115*(41), 10293–10298.

Leconte, J., Forget, F., Charnay, B., Wordsworth, R., & Pottier, A. (2013). Increased insolation threshold for runaway greenhouse processes on earth-like planets. *Nature*, *504*(7479), 268–271.

Manners, J., Edwards, J. M., Hill, P., & Thelen, J.-C. (2017). *SOCRATES: Suite of Community RAdiative Transfer codes based on Edwards and Slingo* (Tech. Rep.). Exeter, UK: UK Met Office.

Meraner, K., Mauritsen, T., & Voigt, A. (2013). Robust increase in equilibrium climate sensitivity under global warming. *Geophysical Research Letters*, *40*(22), 5944–5948.

Pierrehumbert, R. T. (1995). Thermostats, radiator fins, and the local runaway greenhouse. *Journal of the atmospheric sciences*, *52*(10), 1784–1806.

Pierrehumbert, R. T., Brogniez, H., & Roca, R. (2007). On the relative humidity of the atmosphere. *The global circulation of the atmosphere*, *143*, 185.

Popp, M., Schmidt, H., & Marotzke, J. (2016). Transition to a moist greenhouse with CO2 and solar forcing. *Nature communications*, *7*(1), 1–10.

Romps, D. M. (2020). Climate sensitivity and the direct effect of carbon dioxide in a limited-area cloud-resolving model. *Journal of Climate*, *33*(9), 3413–3429.

Russell, G. L., Lacis, A. A., Rind, D. H., Colose, C., & Opstbaum, R. F. (2013). Fast atmosphere-ocean model runs with large changes in CO2. *Geophysical Research Letters*, *40*(21), 5787–5792.

Seeley, J. T., & Jeevanjee, N. (2021). H2O windows and CO2 radiator fins: A clear-sky explanation for the peak in equilibrium climate sensitivity. *Geophysical Research Letters*, *48*(4), e2020GL089609.

Seeley, J. T., Jeevanjee, N., & Romps, D. M. (2019). Fat or fitt: Are anvil clouds or the tropopause temperature invariant? *Geophysical Research Letters*, *46*(3), 1842–1850.

Thomson, S. I., & Vallis, G. K. (2019). The effects of gravity on the climate and circulation of a terrestrial planet. *Quarterly Journal of the Royal Meteorological Society*, *145*(723), 2627–2640.

Vallis, G. K. (2017). *Atmospheric and oceanic fluid dynamics* (2nd ed.). Cambridge, U.K.: Cambridge University Press.

Vallis, G. K., Colyer, G., Geen, R., Gerber, E., Jucker, M., Maher, P., ... Thomson, S. I. (2018). Isca, v1. 0: A framework for the global modelling of the atmospheres of earth and other planets at varying levels of complexity. *Geoscientific Model Development*, *11*(3), 843–859.

Wolf, E., Haqq-Misra, J., & Toon, O. (2018). Evaluating climate sensitivity to CO2 across earth's history. *Journal of Geophysical Research: Atmospheres*, *123*(21), 11–861.

Wolf, E., & Toon, O. (2015). The evolution of habitable climates under the brightening sun. *Journal of Geophysical Research: Atmospheres*, *120*(12), 5775–5794.

Zhang, Y., Jeevanjee, N., & Fueglistaler, S. (2020). Linearity of outgoing longwave radiation: From an atmospheric column to global climate models. *Geophysical Research Letters*, *47*(17), e2020GL089235.

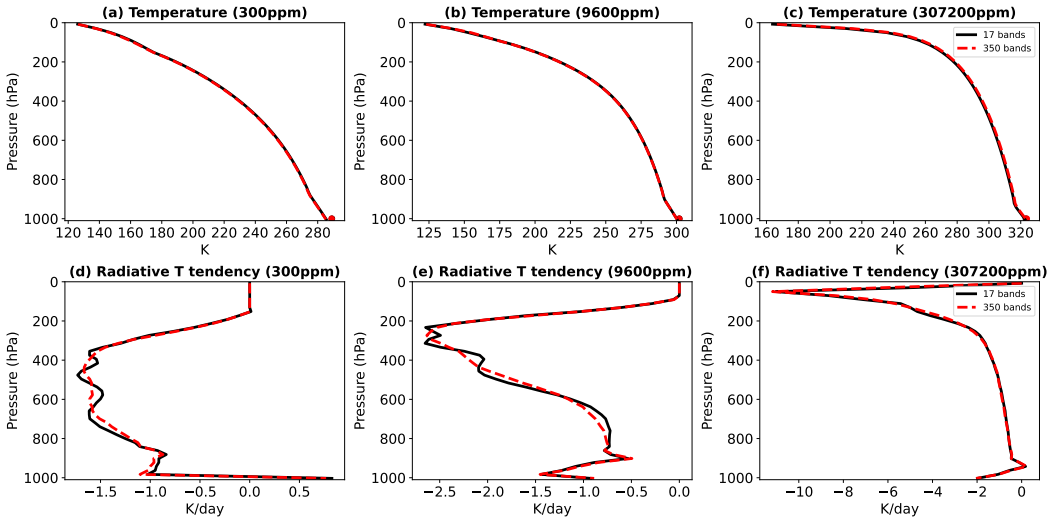

Figure S1. Comparison of temperature and radiative temperature tendency with the lower resolution radiation scheme (17 bands) and the higher resolution radiation scheme (350 bands) in a single column model setting for 300 ppm, 9600 ppm, and 307200 ppm.

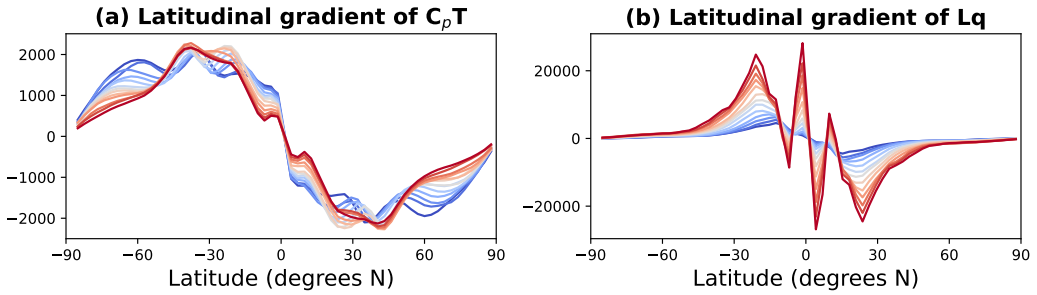

Figure S2. Latitudinal gradient of moist static energy for the dry (a) and moist (b) components for all simulations.

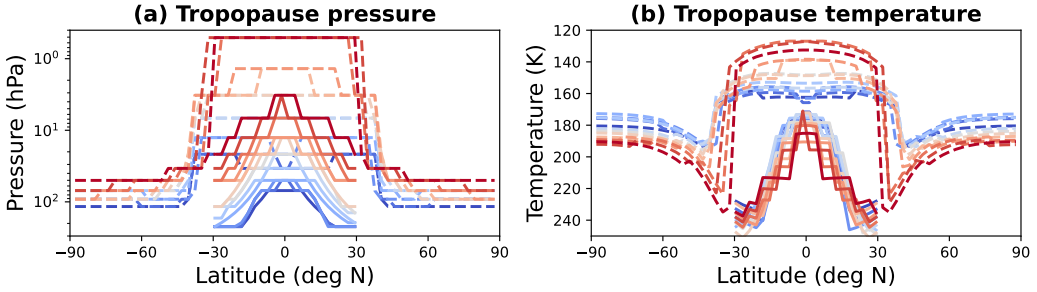

Figure S3. Tropopause pressure (a) and temperature (b) calculated based on the convective criterion (solid) and on a 2K/km threshold (dashed), for all simulations.